

## PRECLINICAL REPORTS

# Low-intensity cold atmospheric plasma reduces wrinkles on photoaged skin through hormetic induction of extracellular matrix protein expression in dermal fibroblasts

Ga Ram Ahn MD, PhD<sup>1</sup>  | Hyung Joon Park BSc<sup>2</sup>  | Young Gue Koh MD<sup>1</sup>  |  
 Sun Hye Shin MD<sup>1</sup>  | Yu Jin Kim MSc<sup>1</sup>  | Min Gyo Song BSc<sup>3</sup>  |  
 Jung Ok Lee PhD<sup>1</sup>  | Hyuck Ki Hong<sup>4</sup> | Kyu Back Lee MD, PhD<sup>2,3</sup>  |  
 Beom Joon Kim MD, PhD<sup>1</sup> 

<sup>1</sup>Department of Dermatology, Chung-Ang University College of Medicine, Seoul, Korea

<sup>2</sup>Department of Interdisciplinary Bio/Micro System Technology, College of Engineering, Korea University, Seoul, Korea

<sup>3</sup>School of Biomedical Engineering, Korea University, Seoul, Korea

<sup>4</sup>Human IT Convergence System R&D Division, Korea Electronics Technology Institute, Seongnam-Si, Gyeonggi-do, Korea

## Correspondence

Kyu Back Lee, MD, PhD, Department of Interdisciplinary Bio/Micro System Technology, College of Engineering, Korea University, 145, Anam-ro, Seongbuk-gu, Seoul 02841, Korea.  
 Email: [kblee@korea.ac.kr](mailto:kblee@korea.ac.kr)

Beom Joon Kim, MD, PhD, Department of Dermatology, Chung-Ang University Hospital, 102, Heukseok-ro, Dongjak-gu, Seoul 06973, Korea.  
 Email: [beomjoon74@gmail.com](mailto:beomjoon74@gmail.com)

## Funding information

Institute for Information and Communications Technology Promotion, Grant/Award Number: 2021-0-01074

## Abstract

**Background:** Recent evidence indicates that cold atmospheric plasma (CAP) can upregulate the production of extracellular matrix (ECM) proteins in dermal fibroblasts and enhance transdermal drug delivery when applied at a low intensity.

**Objectives:** The aim of this study was to evaluate the effect of low-intensity CAP (LICAP) on photoaging-induced wrinkles in an animal model and the expression profiles of ECM proteins in human dermal fibroblasts.

**Methods:** Each group was subjected to photoaging induction and allocated to therapy (LICAP, topical polylactic acid (PLA), or both). The wrinkles were evaluated via visual inspection, quantitative analysis, and histology. The expression of collagen I/III and fibronectin was assessed using reverse transcription-quantitative polymerase chain reaction, western blot analysis, and immunofluorescence. The amount of aqueous reactive species produced by LICAP using helium and argon gas was also measured.

**Results:** Wrinkles significantly decreased in all treatment groups compared to those in the untreated control. The differences remained significant for at least 4 weeks. Dermal collagen density increased following LICAP and PLA application. LICAP demonstrated a hormetic effect on ECM protein expression in human dermal fibroblasts. The production of reactive species increased, showing a biphasic pattern, with an initial linear phase and a slow saturation phase. The initial linearity was sustained for a longer time in the helium plasma (~60 s) than in the argon plasma (~15 s).

**Conclusion:** LICAP appears to be a novel treatment option for wrinkles on the photodamaged skin. This treatment effect seems to be related to its hormetic effect on dermal ECM production.

## KEYWORDS

cold atmospheric plasma, collagen, fibronectin, hormesis, wrinkle

## INTRODUCTION

Wrinkles are one of the most prominent features of photoaged skin.<sup>1</sup> Ultraviolet (UV) irradiation is largely responsible for causing wrinkles because it negatively alters the quality and quantity of extracellular matrix proteins, such as collagen and fibronectin, by causing the overproduction of reactive oxygen (ROS) and nitrogen (RNS) species.<sup>2</sup>

Dermatologists have attempted to meet patients' demands to improve wrinkled skin.<sup>3</sup> A variety of energy-based devices (EBD), injectables, and topical agents are being used to overcome unwanted wrinkles. However, each treatment option has limitations; conventional EBDs inevitably incorporate physical damage by stimulating dermal cells; injectables cause pain during the injection; topical agents, on the other hand, are the gentlest option but still lack sufficient permeability to reach the dermis.

Physical plasma, which is the fourth state of matter, contains both ionized gas molecules and electrons.<sup>4</sup> Ionized gas molecules in physical plasma are highly electrophilic and produce radicals and reactive oxygen and nitrogen species (RONS) in ambient air or living tissues. Therefore, cold atmospheric plasma (CAP) devices can be used effectively for the selective elimination of oxidative stress-vulnerable cells, such as cancer cells, or pathologic microorganisms.<sup>4</sup> Meanwhile, a growing body of evidence suggests that CAP can induce skin rejuvenation by upregulating the production of extracellular matrix proteins at low densities.<sup>5-9</sup> The authors explained this ironic phenomenon with *hormesis*, a term indicating the dose-response relationship phenomenon characterized by low-dose stimulation and high-dose inhibition.<sup>10</sup> Studies that subdivided plasma doses have demonstrated that plasma exhibits a hormetic

effect on fibroblasts; a low dose of plasma appears to be more beneficial than a high dose.<sup>5,7,9</sup> However, it is not yet known whether these effects lead to gross wrinkle improvement in the photoaged skin of living organisms.

Therefore, this study evaluated the effect of low-intensity CAP (LICAP) on wrinkle improvement in photoaged skin using an animal model. Moreover, the expression profiles of collagen and fibronectin, the main protein components of the dermis, were evaluated after a fine subdivision of plasma doses. Based on the drug delivery-enhancing effect of CAP, the benefit of concurrent therapy with topical application of a rejuvenation-boosting agent was also investigated.

## MATERIALS AND METHODS

### Ethics approval

The present study was performed in accordance with the guidelines of the Laboratory Animal Care of the National Institutes of Health, and the experimental protocols were approved by the Chung-Ang University Institutional Animal Care and Use Committee (IACUC, No. 201900124).

### LICAP device and treatment application

The helium plasma jet device used in this study was developed by AGNES Medical Co., Ltd. (Figure 1A,B). N50 (99.999%) helium gas was used as the plasma vehicle gas with a gas flow rate 0.12 L/min. Physical plasma was generated using a 12 kHz radiofrequency with 1000 W power (peak voltage of 6 kV). For the in vivo study, the plasma jet was directly discharged onto the dorsal skin of

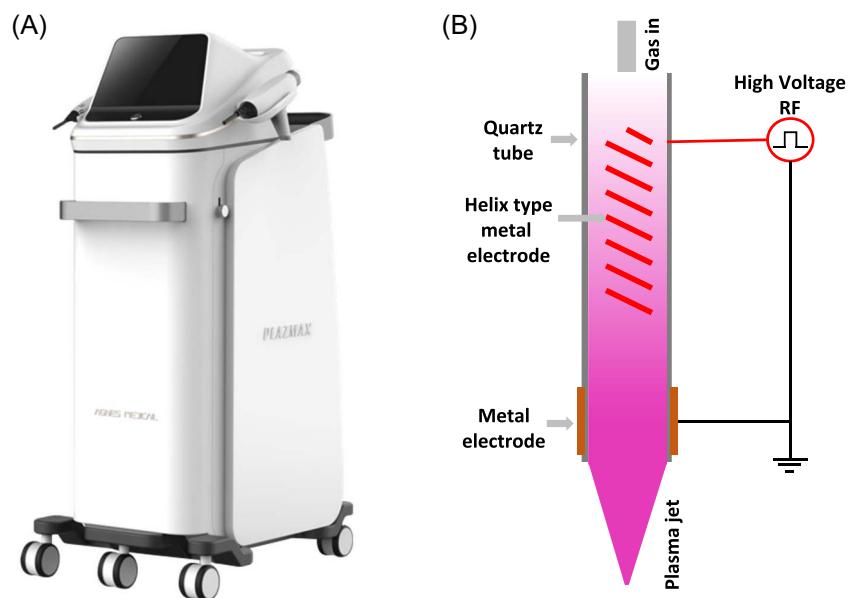


**FIGURE 1** Treatment device. (A) The exterior of the device. (B) Scheme describing the plasma-generating part with a helical-shaped RF electrode.

the mouse for 1 min per treatment session. For the in vitro study, plasma was applied indirectly to the subject cells through plasma-activated media (PAM), which was prepared by a plasma jet application to 3 ml Dulbecco's modified Eagle's medium in 24-well plates at 8 mm height for 5, 10, 15, 20, 25, and 30 s. After subculturing ( $5 \times 10^5$  cells, 80% growth) in four sets of six-well plates, each medium was replaced with each PAM as allocated. The cells were collected 24 h after plasma treatment for analysis.

## Polylactic acid solution

Polylactic acid (PLA) solution was provided by Vaim Co., Ltd. The solution was specifically designed for enhanced transdermal penetration and contained PEGylated PLA nanoparticles (1.5% w/v), loaded with poly DL-lactic acid (1.5% w/v) and 2000 kDa noncrosslinked hyaluronic acid (1.0% w/v). PLA solution (100  $\mu$ l) was applied topically to the dorsal skin of the mice.

## Animal model for in vivo study

Male hairless mice (HRM1; Saeron Bio Inc.) were used in the study after being housed under constant conditions, with a humidity of  $55 \pm 10\%$ , a temperature of  $23 \pm 2^\circ\text{C}$ , and a light cycle of 12 h night/12 h day for 7 days.

## In vivo study design

Mice were divided into five groups of eight mice each (Figure 2). The control group was not subjected to photoaging induction or photoaging treatment. The untreated group was subjected to photoaging but did not receive any plasma treatment. The treatment groups, which consisted of the LICAP treatment group, PLA treatment group, and a concurrent treatment (LICAP + PLA) group, respectively, were subjected to photoaging induction. To induce photoaging, a 312 nm ultraviolet B (UV-B) light was irradiated on the dorsal skin of the hairless mice, with

gradually increasing doses from 30 to 70 mJ/cm<sup>2</sup>, using an automated UV irradiation system (Bio-Spectra, Vilber Corp.). Each allocated treatment (LICAP, PLA, or both) was applied three times a week to each group for 4 weeks ("costimulation period"). After all treatments were discontinued, the changes were observed for another 4 weeks ("treatment-off period") to observe the persistence of the treatment effects. UV-B irradiation was continued (70 mJ/cm<sup>2</sup>, three times a week) throughout the 8 weeks of the costimulation and following treatment-off periods.

## Efficacy evaluation

Gross magnified images and three-dimensional (3D) microstructure of the dorsal skin were obtained with a phototrichogram (Folliscope 4.0, LeadM) and an optical 3D skin measurement system (PRIMOS Lite, GFMe-stechnik GmbH), respectively. Each measurement was performed weekly during the study period.

To perform the quantitative analysis, wrinkle levels were converted into numeric values using an optical 3D skin measurement system. Ra (average of all heights and depths to the reference plane) and Rmax (maximum peak-to-valley roughness height) values were used as the main parameters to represent the wrinkle levels.

The decrement percentage of Ra or Rmax values at a specific moment (*i*) from the baseline (DPR<sub>a<sub>i</sub></sub> or DPR<sub>max<sub>i</sub></sub>) was calculated using the following equation:

$$\begin{aligned} \text{DPR}_{a_i} (\%) &= \frac{(\text{mean Ra at week 0} - \text{mean Ra at week } i)}{\text{mean Ra at week 0}} \\ &= \frac{\text{Ra}_0 - \text{Ra}_i}{\text{Ra}_0} \end{aligned}$$

To perform a histological examination, the biopsy samples obtained from the dorsal skin of the hairless mice were fixed with 10% formalin for 12 h, embedded in paraffin wax, and sectioned into 5  $\mu$ m slices. After staining the sections with hematoxylin and eosin and Masson's trichrome, the patterns of changes in the skin tissue were observed under an optical microscope

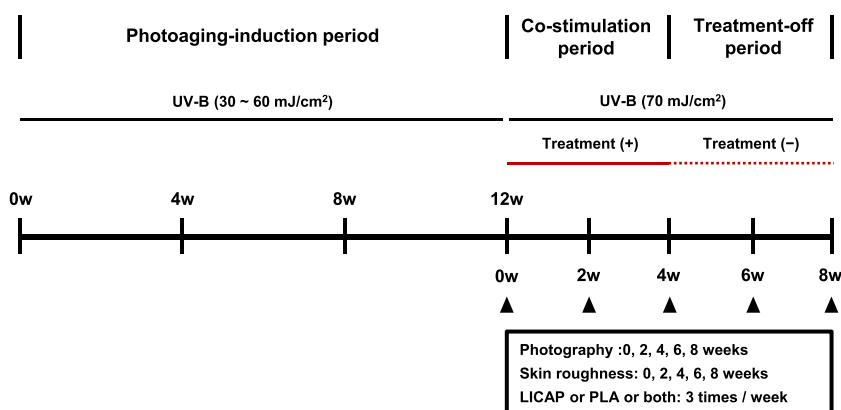


FIGURE 2 Study design scheme.

( $\times 200$  magnification, DM750, Leica). Changes in epidermal thickness were quantified using a slide-viewing application (3DHISTECH Ltd.). Epidermal thickness was defined as the vertical distance between the upper margin of the stratified epithelium and the basement membrane.

### Hs68 cell culture for in vitro study

Human primary foreskin fibroblasts (HS-68, American Type Culture Collection) were grown in Dulbecco's modified Eagle's medium supplemented with 10% fetal bovine serum (FBS) (Thermo Fisher Scientific) and 1% penicillin–streptomycin (10 000 units and 10 mg/mL, respectively; Thermo Fisher Scientific) and incubated at 37°C in a humidified chamber containing 5% CO<sub>2</sub>. The number of passages for the cell culture ranged from 3 to 10.

### Cell viability test

The cell viability was quantified using a colorimetric WST-1 assay. Hs68 cells ( $1.5 \times 10^5$ /ml) were seeded in 96-well plates and incubated at 37°C in a humidified chamber containing 5% CO<sub>2</sub>. After 24 h, 10  $\mu$ l of WST reagent was added. The spectrophotometric absorbance was measured at a wavelength of 450 nm.

### Reverse transcription-quantitative polymerase chain reaction assay for mRNA quantitation (RT-qPCR)

RNA from Hs68 cells was extracted using the TRIzol reagent (Invitrogen). The target RNA was reverse-transcribed into cDNA using qPCR 2 $\times$  PreMIX SYBR (Enzynomics). The denaturation process lasted 10 min at 95°C, and PCR thermocycling was as follows: 40 cycles of 10 s at 95°C, 15 s at 60°C, and 30 s at 72°C. The results were calculated as cycle Ct values using the GAPDH gene expression assay. Each purified mRNA (signal intensity of 1.8–2.0 under 260/280 nm fluorescence excitation/emission wavelengths) was quantified using a spectrophotometer (NanoDrop™; Thermo Fisher Scientific). Detailed information regarding the process of the RT-qPCR assay is presented in the Supporting Information Data according to the minimum information for publication of quantitative PCR experiments (MIQE précis) (Supporting Information: Supplement 1).<sup>11</sup>

### Western blot analysis

The cells were cultured for 24 h in a medium to which FBS was added. After removing the FBS, the treated medium was replaced by the test medium. Cell lysates were centrifuged at 13 000g for 20 min at 4°C. The supernatant

was recovered, and the protein concentration was measured using the Bio-Rad reagent. Samples of the same concentration were separated by electrophoresis on a 10% sodium dodecyl sulfate-polyacrylamide gel electrophoresis gel. The gel was blotted onto a membrane, which blocked with 5% skim milk in Tris-buffered saline and Tween 20 and incubated for 24 h. The blotted membranes were incubated overnight at 4°C with the following primary antibodies: antifibronectin (ab2413; Abcam Plc.), anticollagen type I (ab138492), anticollagen type III (ab7778), and anti- $\beta$ -actin (control, sc-47778; Santa Cruz Biotechnology, Inc.). After washing, the membranes were incubated with secondary antibodies (horseradish peroxidase-conjugated anti-mouse or anti-rabbit antibody; Vector Labs, Inc.) for 2 h. After washing, protein expression was detected using enhanced chemiluminescence detection reagents (Pierce Biotechnology).

### Immunocytochemistry study

Cells cultured in four-chamber glass slides were fixed with 4% paraformaldehyde at room temperature (20–22°C) for 10 min. Fixed cells were permeabilized with 0.1% Triton X-100 for 10 min, washed twice with phosphate-buffered saline, and blocked with 2% bovine serum albumin for 10 min. The four-chamber glass slides were incubated with the following antibodies: antifibronectin (ab2413) for 24 h and goat anti-rabbit immunoglobulin G (IgG; Alexa Flour 488; ab150077) for 1 h. After applying DAPI mounting solution for 30 min, the cells were analyzed using a fluorescence microscope (Olympus Optical) at  $\times 40$  magnification.

### Quantification of collagen production

Image threshold analysis software (ImageJ, National Institutes of Health) was used to quantify the amount of collagen marked in the Masson's trichrome and immunocytochemistry assays. Image processing and analysis were performed according to the previously established protocols.<sup>12,13</sup> The quantitative analysis was based on the color density values measured among five independent square areas with a side length of 100  $\mu$ m. The RGB (red, green, and blue) colors of the sample images were deconvoluted. The blue component for Masson's trichrome staining and green component for the immunocytochemistry assay were used for quantification. The arbitrary unit was defined as the value obtained by dividing the color density in each group by that in the normal control group.

### Quantification of reactive species production

To quantify the reactive species, plasma was induced in 3 ml phosphate-buffered saline in a 12-well plate at an

8 mm height for 5, 10, 15, 30, 60, and 120 s. Argon and helium gas, the two most commonly used noble gases for plasma jet generation in medical applications, were used as vehicle gases for comparison. The other treatment conditions associated with plasma generation in the device were the same as those used in the *in vivo* investigations. The amount of aqueous reactive species produced in the target solution was measured using a RONS assay kit (OxiSelect™, Cell Biolabs Inc.) following the manufacturer's instructions. A 2',7'-dichlorodihydrofluorescein (DCF) standard curve was used to quantify reactive species production. Briefly, 50 µl of the catalyst was added to the sample, and 100 µl of DCF solution was added to the sample and incubated for no more than 20 min. The fluorescence emitted from the redox reaction in the solution was measured using a plate reader (Gemini EM; Molecular Devices) at 480/530 nm excitation.

### Statistical analysis

A one-way ANOVA followed by Tukey's multiple comparisons and Student's *t*-test were used to detect and determine significant differences between each treatment group and the untreated control (GraphPad Prism 7.0). For the *t*-test, the Shapiro–Wilk test was used to confirm whether the sample populations were normally distributed. All experiments were performed in triplicate, and all data are expressed as mean ± SD. Each mean difference was considered significant when the *p* value was <0.05.

## RESULTS

### Impact of LICAP treatment on cell viability and body weight

The WST-1 assay and body weight measurements were performed to evaluate safety. The data from the WST-1 assay showed no significant change in viability between the groups during the entire observation period (Supporting Information: Supplement 2A). Body weight did not show any significant changes during the study period (Supporting Information: Supplement 2B).

### LICAP and PLA treatments visually improved the UV-induced wrinkles

Visual inspections were performed on magnified images obtained from the phototrichogram (Figure 3A) and the optical 3D skin measurement system (Figure 3B,C). After 4 weeks of costimulation, the treatment groups showed an improvement with regard to the UV-induced wrinkles whereas the untreated group did not. During

the 4-week treatment-off period, the wrinkles slowly began to reappear after the UVB irradiation. Among the treatment groups, the treatment effect and its persistence seemed exhibited the best in the concurrent therapy (LICAP + PLA) group. For this group, no specific skin lesions were detected via visual inspection during the treatment period, with the exception of photoaging-related wrinkles.

### Surface roughness improvements via LICAP and PLA treatments

A quantitative analysis of wrinkle severity was performed based on the data from the optical 3D skin measurement system (Figure 4A,B and Tables 1 and 2). The photoaging induction in this study was deemed to be valid based on the significant differences in Ra and Rmax values between the normal and untreated control groups during the treatment period. During the costimulation period (Weeks 0–4), the mean Ra and Rmax values gradually decreased in the treatment groups. The mean Ra and Rmax values of the three treatment groups were lower than those of the untreated group during most of the study period (costimulation period + treatment-off period). The differences were significant between the concurrent treatment group (LICAP + PLA) and the untreated group from Week 1 onwards. The LICAP and PLA groups showed significantly lower Ra and Rmax values than the untreated control from Week 2 onwards. These differences persisted at the end of the treatment period (~Week 8).

The decrement percentage of the mean Ra or Rmax value at a specific moment (*i*) from baseline,  $DPRa_i$  and  $DPRmax_i$  are presented as line graphs to clearly visualize the changes in wrinkle improvement over time (Figure 5A,B). The  $DPRa_i$  and  $DPRmax_i$  values of the three treatment groups (LICAP, PLA, and LICAP + PLA) gradually increased during the costimulation period. These improvements diminished during the treatment-off period but were still markedly higher than those of the untreated group. At Week 4, the end of the costimulation period,  $DPRa_4$  and  $DPRmax_4$  were the most remarkable in the LICAP + PLA group (30.8% and 37.4%), followed by that in the LICAP group (23.5% and 28.1%) and the PLA group (22.8% and 20.5%). At Week 8, the end of the treatment-off period,  $DPRa_8$  and  $DPRmax_8$  were 23.1% and 25.1% in the LICAP + PLA group, 24.1% and 23.0% in the LICAP group, and 13.8% and 11.3% in the PLA group.

### Histologic changes after treatment administration

Skin biopsies were performed to investigate the histological changes in the treated skin (Figure 6A–C). The data

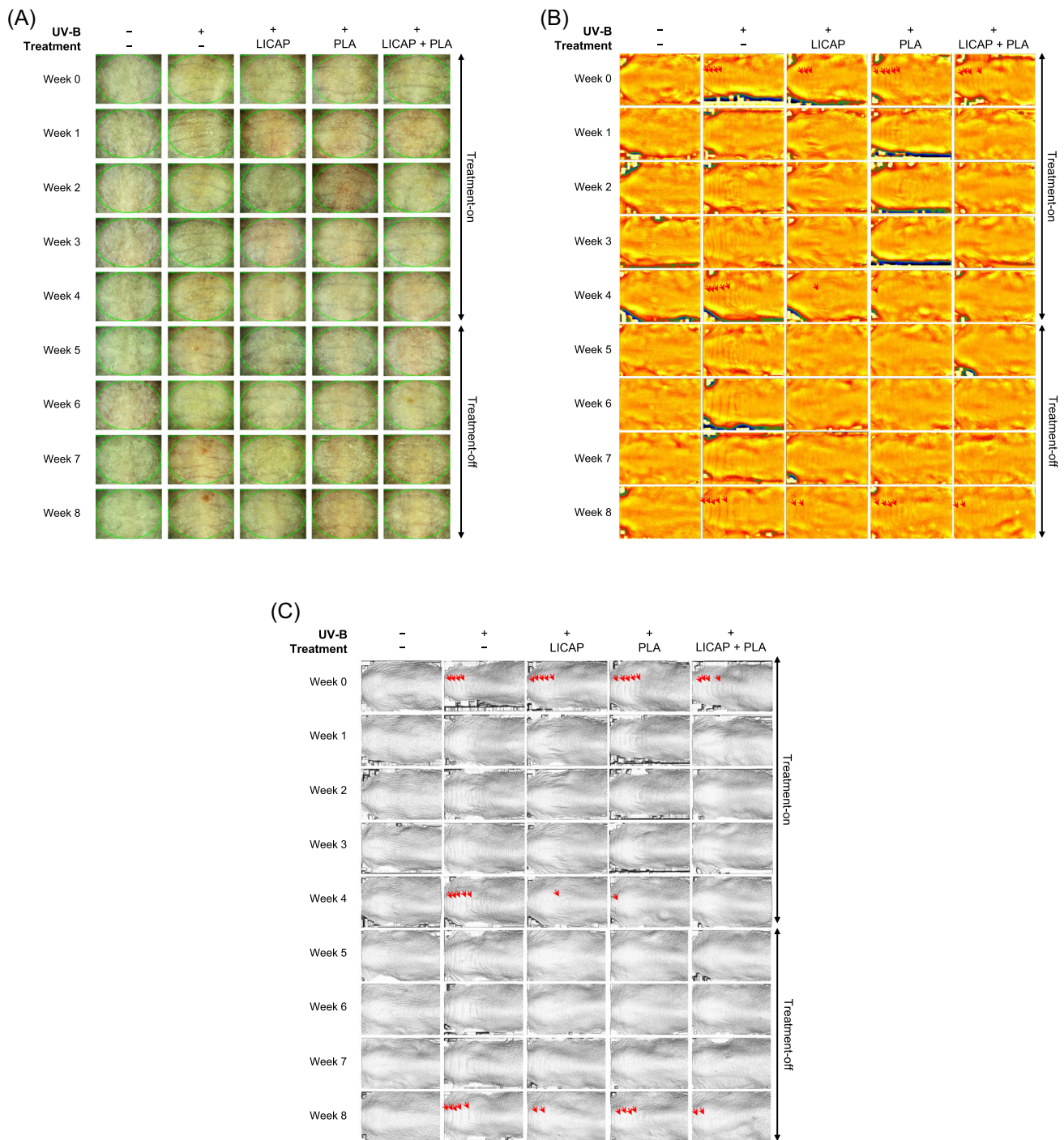


**FIGURE 3** Photographs for visual inspection. (A) Phototrichogram image of dorsal skin. (B) Color height maps. (C) three-dimensional (3D) mapping images of dorsal skin obtained from the optical 3D skin measurement system.

from the histological examination showed a marked decrease in collagen density and an increase in epidermal thickness in the untreated skin compared to those of the normal control group, suggestive of the photoaging effects of UV-B irradiation (Figure 6A). In the treatment groups, dermal collagen density was higher than that in the untreated control. Especially at Week 8, the collagen densities of the

treatment groups appeared to be similar to that of the normal control group. The treatment groups exhibited thinner epidermises than did the untreated control. However, the difference in epidermal thickness was not as obvious as that in collagen density.

Collagen density and epidermal thickness, the two main factors that contribute to UV-induced wrinkles, were quantitatively analyzed using an image threshold

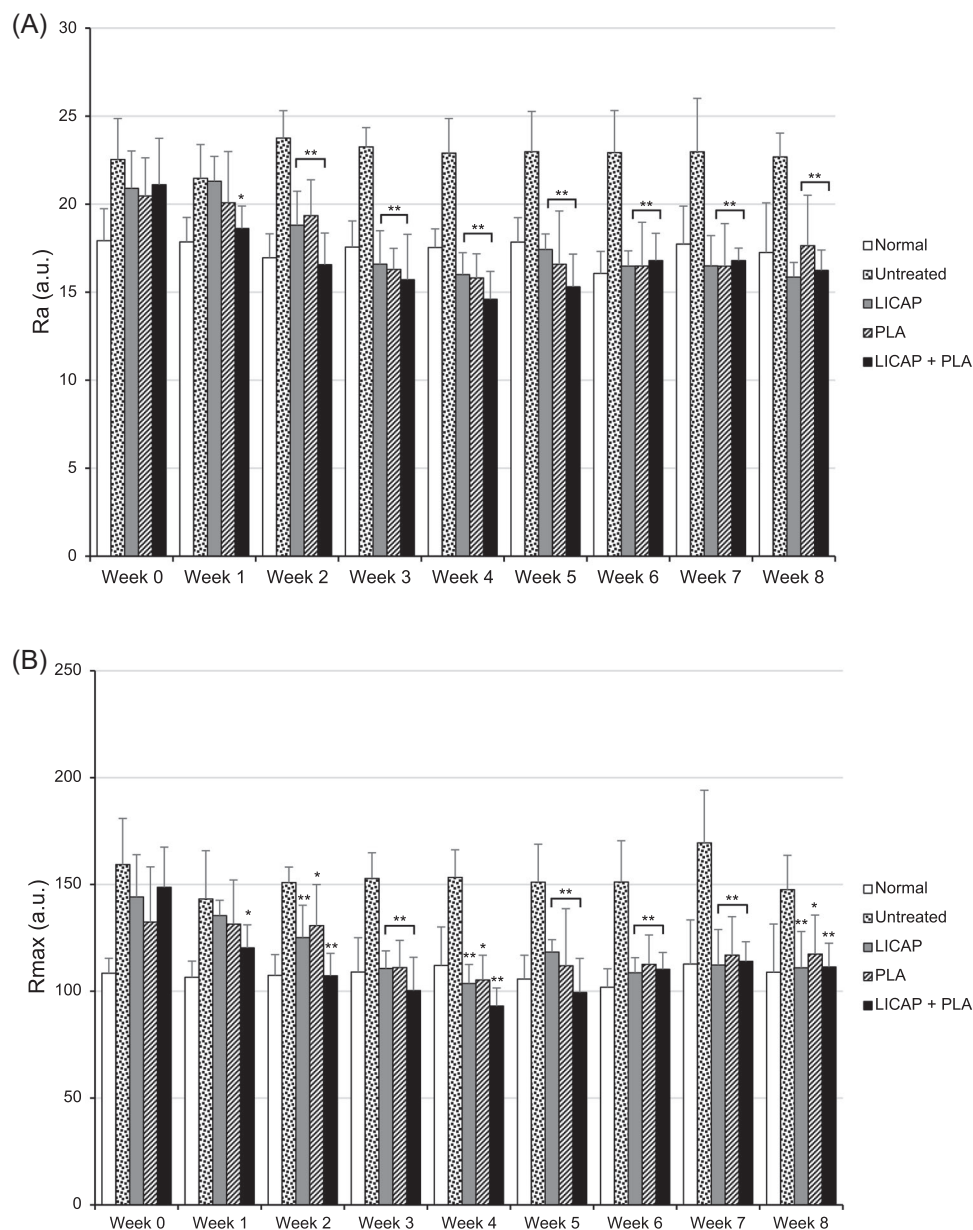


**FIGURE 4** Quantitative analysis of wrinkles on dorsal skin via the three-dimensional skin measurement system. (A) Ra value. (B) Rmax value (\* $p < 0.05$ , \*\* $p < 0.01$ , compared to the untreated group).

analysis software and a slide-viewing application (Figure 6B,C). Owing to UV-B irradiation, the untreated control group showed marked photoaging-associated changes compared to the normal control group; collagen density was significantly lower, and epidermal thickness was significantly higher at Weeks 4 and 8. In contrast, the collagen density of every treatment group was significantly higher than that of the untreated group at Week 8, and epidermal thickness was significantly lower in the treatment groups than in the untreated group. Compared to the epidermal thicknesses, the collagen densities of the treatment groups were closer to those of the normal control group.

### Extracellular matrix expression in human dermal fibroblasts showed a hormetic response to the LICAP treatment

Immunocytochemistry was performed to determine whether the increase in dermal collagen density after plasma irradiation confirmed in histological tests was due to an increased amount of dermal matrix proteins (Figure 7A; Supporting Information: Supplement 3). As a result of subdividing the time of exposure to LICAP, relatively more dermal matrix proteins were expressed in the groups exposed to the plasma for very short times (5 and 10 s) than in groups with a longer duration of plasma exposure. The data from the western

**TABLE 1** Ra values measured via the optical three-dimensional skin measurement system (mean ± SD)

	Week 0	Week 1	Week 2	Week 3	Week 4	Week 5	Week 6	Week 7	Week 8
Control (n = 8)	17.9 ± 1.82	17.9 ± 1.39	17.0 ± 1.36	17.6 ± 1.49	17.5 ± 1.06	17.8 ± 1.39	16.1 ± 1.24	17.7 ± 2.16	17.3 ± 2.82
Untreated control (n = 8)	22.5 ± 2.33	21.5 ± 1.92	23.8 ± 1.55	23.3 ± 1.10	22.9 ± 1.97	23.0 ± 2.29	22.9 ± 2.39	23.0 ± 3.03	22.7 ± 1.35
LICAP (n = 8)	20.9 ± 2.12 (0.195)	21.3 ± 1.41 (0.852)	18.8 ± 1.93** (1.92 × 10 <sup>-4</sup> )	16.6 ± 1.90** (3.58 × 10 <sup>-6</sup> )	16.0 ± 1.25** (4.68 × 10 <sup>-6</sup> )	17.4 ± 0.881** (9.75 × 10 <sup>-4</sup> )	16.5 ± 0.862** (4.74 × 10 <sup>-4</sup> )	16.5 ± 1.72** (0.00318)	15.9 ± 0.834** (1.15 × 10 <sup>-5</sup> )
PLA (n = 8)	20.5 ± 2.16 (0.111)	20.1 ± 2.91 (0.311)	19.4 ± 2.03** (6.62 × 10 <sup>-4</sup> )	16.3 ± 1.20** (8.95 × 10 <sup>-8</sup> )	15.8 ± 1.37** (4.77 × 10 <sup>-6</sup> )	16.6 ± 3.02** (0.00548)	16.5 ± 2.48** (0.00310)	16.5 ± 2.42** (0.00567)	17.6 ± 2.87** (0.00978)
LICAP + PLA (n = 8)	21.1 ± 2.64 (0.304)	18.6 ± 1.28** (0.00661)	16.6 ± 1.79** (3.67 × 10 <sup>-6</sup> )	15.7 ± 2.58** (1.22 × 10 <sup>-5</sup> )	14.6 ± 1.58** (1.59 × 10 <sup>-6</sup> )	15.3 ± 1.86** (3.96 × 10 <sup>-4</sup> )	16.8 ± 1.55** (0.00134)	16.8 ± 0.710** (0.00217)	16.2 ± 1.16** (4.08 × 10 <sup>-5</sup> )

Note: Significance levels of difference between the untreated control and each treatment group are parenthesized (\*p < 0.05, \*\*p < 0.01).

**TABLE 2** Rmax values measured via the optical three-dimensional skin measurement system (mean ± SD)

	Week 0	Week 1	Week 2	Week 3	Week 4	Week 5	Week 6	Week 7	Week 8
Control (n = 8)	108 ± 6.98	107 ± 7.57	107 ± 9.72	109 ± 16.0	112 ± 18.0	106 ± 11.2	102 ± 8.63	113 ± 20.6	109 ± 22.5
Untreated control (n = 8)	159 ± 21.6	143 ± 22.6	151 ± 7.28	153 ± 12.1	153 ± 12.9	151 ± 17.8	151 ± 19.3	169 ± 24.7	148 ± 16.1
LICAP (n = 8)	144 ± 19.8 (0.195)	135 ± 7.15 (0.405)	125 ± 15.1** (0.00160)	111 ± 8.22** (6.06 × 10 <sup>-6</sup> )	104 ± 8.95** (2.40 × 10 <sup>-6</sup> )	118 ± 5.82** (0.00447)	109 ± 7.10** (0.00170)	112 ± 16.6** (0.00262)	111 ± 16.9** (0.00817)
PLA (n = 8)	132 ± 25.8 (0.0561)	131 ± 20.6 (0.331)	131 ± 19.2* (0.0236)	111 ± 12.7** (4.00 × 10 <sup>-5</sup> )	105 ± 11.6** (9.44 × 10 <sup>-6</sup> )	112 ± 26.7* (0.0259)	113 ± 13.8** (0.00659)	117 ± 17.9** (0.00489)	117 ± 18.2* (0.0339)
LICAP + PLA (n = 8)	149 ± 18.8 (0.346)	120 ± 10.8* (0.0327)	107 ± 10.5** (1.06 × 10 <sup>-6</sup> )	100 ± 15.6** (1.37 × 10 <sup>-5</sup> )	93.1 ± 8.44** (2.59 × 10 <sup>-7</sup> )	99.5 ± 15.9** (0.00129)	110 ± 7.86** (0.00232)	114 ± 9.17** (0.00152)	111 ± 11.1** (0.00332)

Note: Significance levels of difference between the untreated control and each treatment group are parenthesized (\*p < 0.05, \*\*p < 0.01).

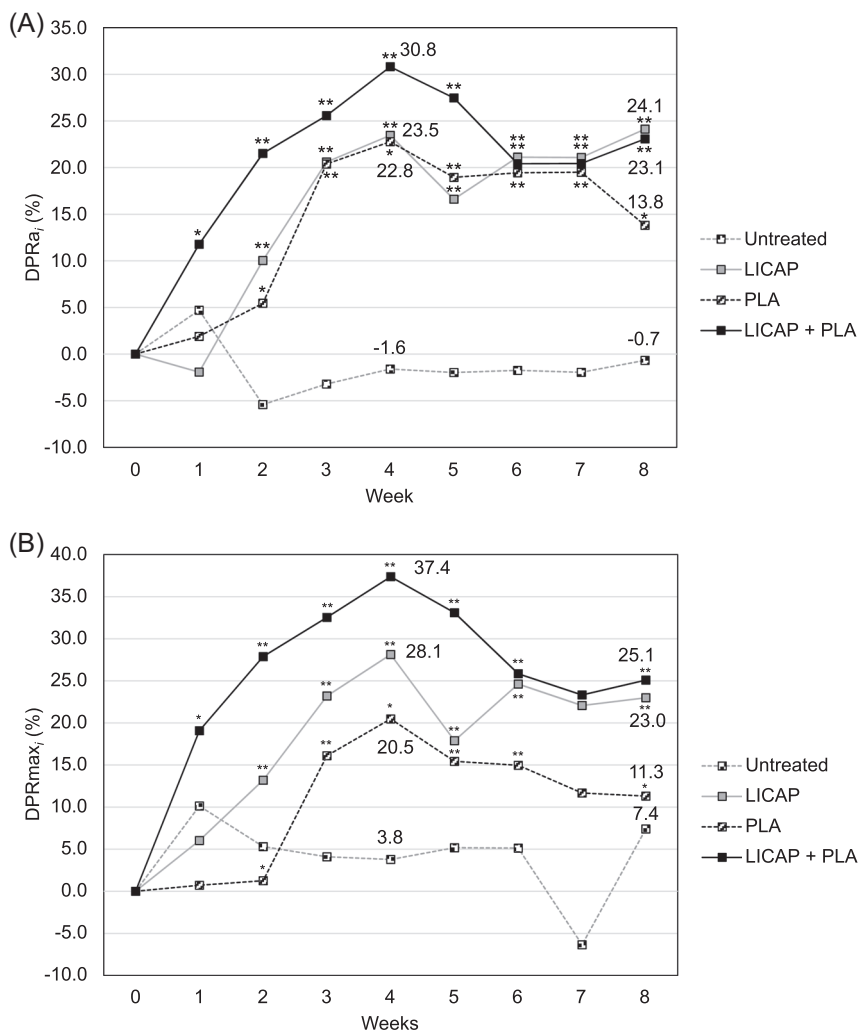


**FIGURE 5** Decrement percentage of mean (A) Ra and (B) Rmax values from Week 0 (\* $p < 0.05$ , \*\* $p < 0.01$ , compared to the untreated group).

blot analysis seemed to correlate with the data from the immunocytochemistry examination; the bands of short-exposure groups (5 and 10 s) were denser than those of the long-exposure groups (Figure 7B; Supporting Information: Supplement 4).

An RT-qPCR was performed to determine whether the change in the amount of dermal matrix proteins was associated with increased endogenous synthesis (Figure 7C). As shown in the immunocytochemistry and western blot data, mRNA expression was significantly increased in the short-exposure group (5 and 10 s), whereas the longer treatment duration groups showed no significant changes.

### Quantification of aqueous reactive species produced via LICAP treatment

A RONS assay using 2',7'-dichlorofluorescein oxidation was performed to estimate the quantity of aqueous reactive species produced via LICAP treatment (Figure 8). The helium plasma produced less RONS than the argon plasma at every treatment time, and the differences were significant from 5 to 30 s ( $p < 0.01$ ;

Figure 8A). Notably, the increasing pattern of RONS production was biphasic in both groups; the initial phase with high linearity was followed by a slow saturating phase (Figure 8B). The initial phase of the helium plasma was longer (0–60 s) than that of argon plasma (0–15 s). The data from both gases were closely fitted to a linear regression line ( $R^2 = 0.9918$  and  $0.9614$ , respectively; Figure 8C,D).

## DISCUSSION

This study evaluated the effects of LICAP on photoaging-induced wrinkles in an animal model and the expression profiles of extracellular matrix proteins in human dermal fibroblasts. LICAP was defined to distinguish the device from other conventional CAP devices that are designed to be used in a destructive manner, such as for skin resurfacing,<sup>14–16</sup> cancer therapy,<sup>17</sup> or tissue coagulation.<sup>18</sup> In this paper, the term *LICAP* indicates a physical plasma device that is designed to tune its plasma effluent intensity in a *low range* to enhance the tissue (or cell) regeneration without damaging its viability.

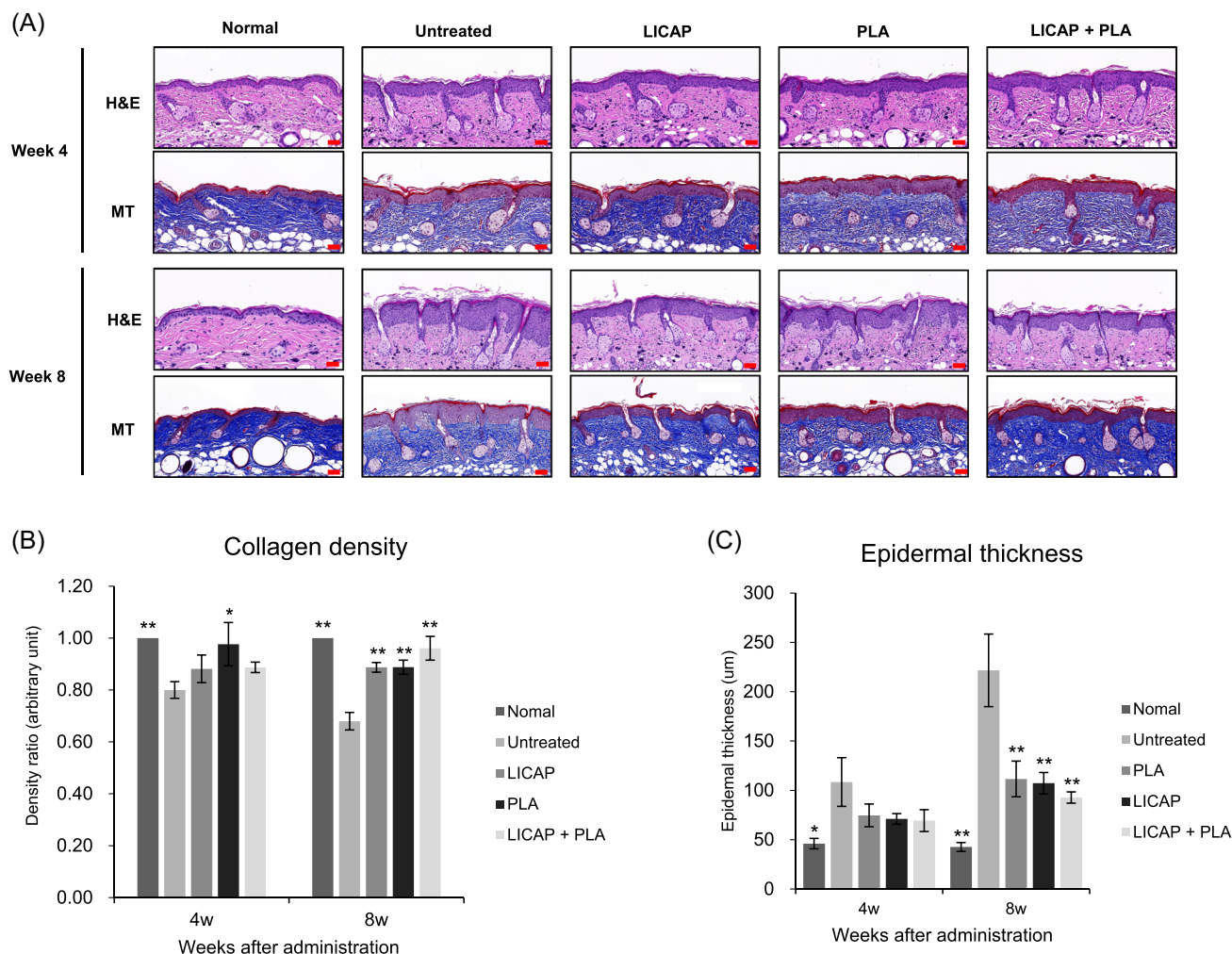


**FIGURE 6** (A) Histologic examination of dorsal skin at Weeks 4 and 8 (hematoxylin & eosin and Masson's trichrome stains,  $\times 200$  magnifications, each scale bar indicates  $100\ \mu\text{m}$ ). Quantitative measurement of collagen density (B) and epidermal thickness (C) via image analysis ( $*p < 0.05$ ,  $**p < 0.01$ , compared with the untreated group).

According to visual inspection, photoaging induced typical changes in photoaged skin (Figure 3A–C). In the treatment groups, UV-induced wrinkles improved after the treatments, of which the effects persisted for 4 weeks post-treatments. The treatment effect and its persistence in the concurrent therapy (LICAP + PLA) group seemed to be the most prominent among the treatment groups.

These visual changes in UV-induced wrinkles after treatment were also evident in the results of the quantitative skin roughness analysis (Figure 4A,B). The differences in the mean Ra and Rmax values between each treatment group and the untreated group were significant for most of the study period (costimulation and treatment-off periods). The differences were significant between the concurrent treatment group (LICAP + PLA) and the untreated group from Week 1 until the end of the study; the LICAP and PLA groups showed significantly lower Ra and Rmax values than the untreated control did from Week 2 onwards.

$\text{DPR}_i$  and  $\text{DPR}_{\text{max}_i}$ , the decrement percentage of the Ra or Rmax value at a specific moment ( $i$ ) from baseline, were useful for visualizing wrinkle improvement over time (Figure 5A,B). The data from the skin roughness measurement suggested that the groups treated with LICAP, topical PLA, and concurrent therapy were able to mitigate the UV-induced wrinkles; the mean Ra value decreased by 23.5% ( $\text{DPR}_{\text{Ra}_4}$ ) after 4 weeks of LICAP treatment ( $\text{DPR}_{\text{max}_4} = 28.1\%$ );  $\text{DPR}_{\text{Ra}_4}$  in the PLA group was 22.8% ( $\text{DPR}_{\text{max}_4} = 20.5\%$ );  $\text{DPR}_{\text{Ra}_4}$  in the LICAP + PLA group was 30.8% ( $\text{DPR}_{\text{max}_4} = 37.4\%$ ).

Moreover, the LICAP and PLA groups seemed to either delay or suppress the reoccurrence of UV-induced wrinkles after discontinuation; in the LICAP group,  $\text{DPR}_{\text{Ra}_8}$  and  $\text{DPR}_{\text{max}_8}$  were 24.1% and 23.0%, respectively;  $\text{DPR}_{\text{Ra}_8}$  and  $\text{DPR}_{\text{max}_8}$  were 13.8% and 11.3% in the PLA group and 23.1% and 25.1% in the LICAP + PLA group, respectively. By contrast, the  $\text{DPR}_{\text{Ra}_8}$  and  $\text{DPR}_{\text{max}_8}$  of the untreated group were  $-0.7\%$  and  $7.4\%$ , respectively.

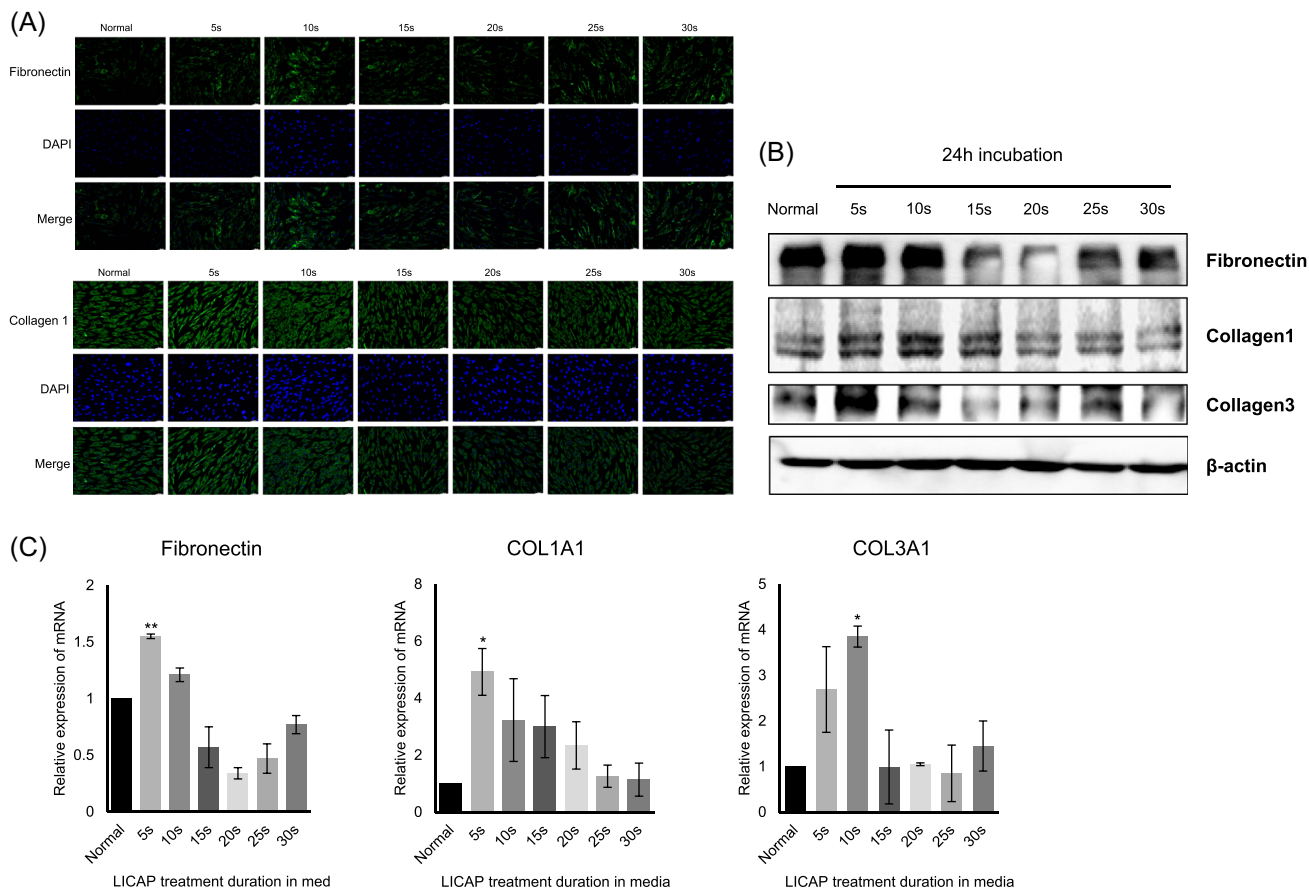


**FIGURE 7** Data from (A) immunocytochemistry, (B) western blot, and (C) reverse transcription quantitative polymerase chain reaction analyses. Expression levels of the main extracellular matrix proteins in human dermal fibroblasts show a hormetic response to the LICAP treatment (\* $p < 0.05$ , \*\* $p < 0.01$  in (C), compared with the untreated group). LICAP, low-intensity cold atmospheric plasma.

These changes in UV-induced wrinkles were also reflected in the histological data (Figure 6A–C). The histological examination revealed that the photoaging induction conducted in this study was effective enough to induce typical changes in photoaging, including decreased collagen density and increased epidermal thickness. These changes were suppressed by the treatments, which was particularly noticeable in collagen density. Hence, the results of the histological analysis suggest that the change in the density of dermal matrix proteins contributed to wrinkle improvement via these treatments.

The *in vitro* studies demonstrated that LICAP had a hormetic effect on the expression of dermal matrix proteins in human dermal fibroblasts; low doses (5 and 10 s) of LICAP significantly upregulated the expression of collagen I/III and fibronectin, whereas higher doses did not (Figure 7A–C). This result is consistent with those of previously reported studies that observed the hormetic effect of CAP.<sup>19,20</sup> Recently, Hwang et al.<sup>7</sup> suggested that low-dose CAP could be used to treat wrinkles based on the mechanism of hormesis. The authors' *in vitro* study revealed that this treatment

upregulated collagen production in human dermal fibroblasts. Moreover, they found that the treatment demonstrated interesting antiaging effects on UV-irradiated human dermal fibroblasts, such as the activation of antioxidant transcription factors, including nuclear factor erythroid 2-related factor 2 (Nrf2), the upregulation of levels of endogenous cytoprotective proteins (sirtuin 1 and heme oxygenase 1 [HO-1]), the attenuation of intracellular RONS accumulation, the inhibition of cellular senescence via p53 activation, and the stabilization of mitochondrial potential.

According to recent studies, the hormetic effect induced by LICAP treatment seems to be related to activation of the Nrf2/antioxidant response element (ARE) pathway.<sup>19–24</sup> Through this mechanism, a mild elevation of intracellular oxidative stress induced by LICAP upregulates the cellular endogenous antioxidant buffering capacity<sup>21,22,25–28</sup> and induces selective autophagy.<sup>29–32</sup> Kelch-like ECH-associated protein 1 (Keap1), which is consistently expressed in the cytoplasm, sequesters the Nrf2, a transcription factor for various endogenous antioxidants.<sup>27,33</sup> As a sensor protein for oxidative stress, Keap1 is sensitive to increased levels of

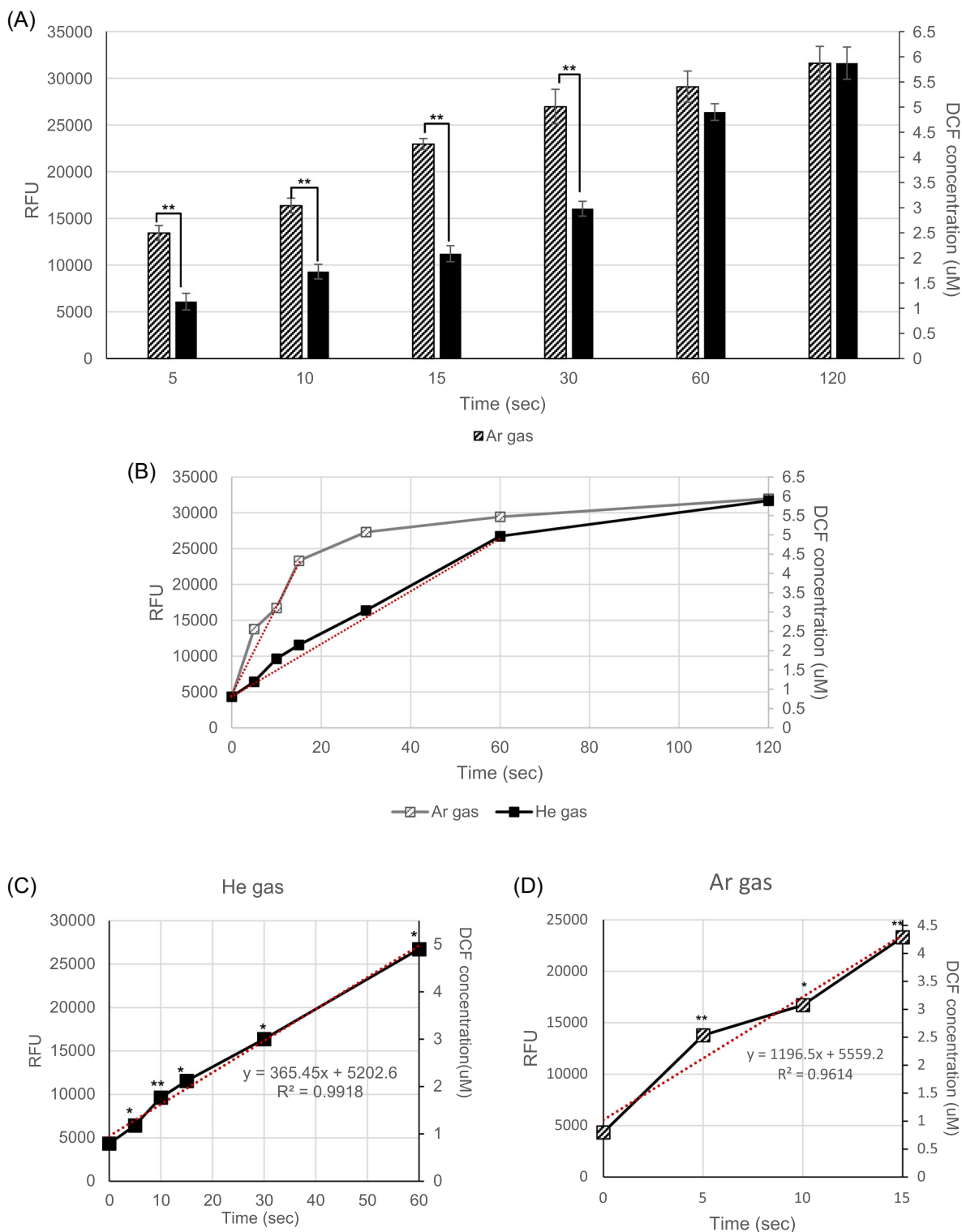


**FIGURE 8** Quantification data for the aqueous reactive species production. (A) RONS production by time in helium and argon plasma. Note the significant differences between vehicle gases from 5 to 30 s. (B) Time-scaled RONS production curves using helium and argon plasma. (C, D) Initial linearly increasing phases of the RONS production curves of helium and argon plasma. Statistical significance was measured by comparison between the previous time and the present ( $*p < 0.05$ ,  $**p < 0.01$ . RFU, relative fluorescence units. DCF, 2',7'-dichlorodihydrofluorescein); RONS, reactive oxygen and nitrogen species.

reactive species (ROS, RNS, or free radicals) through its cysteine residues.<sup>26,34</sup> When the sensor cysteine residues are oxidized by reactive species, Nrf2 is released from Keap1 and translocated into the nucleus.<sup>28</sup> Nrf2 then binds to the ARE sequence on the nuclear DNA and upregulates the expression of a variety of Phase 2 antioxidant proteins, such as NAD(P)H:quinone oxidoreductase 1 (NQO1), glutathione *S*-transferase subunit  $\gamma$  (GST  $\gamma$ ), gamma-glutamylcysteine synthetase ( $\gamma$ -GCS), and HO-1 to increase the cellular antioxidant buffer capacity.<sup>35,36</sup> The activation of Nrf2 also triggers selective autophagy by upregulating the expression of p62, a key adaptor substrate protein for selective autophagy.<sup>29</sup> Moreover, p62 competitively inhibits Keap1, allowing Nrf2 to remain activated. In other words, p62 and Nrf2 form a positive feedback loop upon activation.<sup>30–32</sup>

Interestingly, concurrent therapy (LICAP + PLA) showed an additive effect on wrinkle improvement. The effect of LICAP was augmented by topical PLA application, which is a widely used injectable material to stimulate collagen synthesis in the dermis.<sup>37–44</sup> The additive effect of concurrent therapy is likely related to the ability of CAP to enhance transdermal drug delivery via transcellular and intercellular routes.<sup>45</sup> CAP enhances the transcellular route by increasing the permeability of the plasma membrane through the peroxidation of lipid components in the phospholipid bilayer.<sup>46–51</sup> CAP also enhances intercellular delivery by suppressing the expression of cell adhesion molecules, such as E-cadherin.<sup>37,52</sup>

Our quantification analysis confirmed that the LICAP device used in the present study could precisely adjust the reactive species production in the target solution (Figure 8A–D). Choosing helium over argon as a vehicle gas is an easier way to designate a therapeutic range because it produces reactive species at a lower level (Figure 8A) and in a gentler manner (Figure 8B–D). This is because helium has the highest ionization energy among the vehicle gases commonly used for generating plasma jets. Under the same plasma-generating condition, the output plasma density from the helium plasma jet is lower than that of the others because the helium atom has the lowest chance of being ionized.<sup>53</sup>

Understandably, the “therapeutic window” is an important concept in LICAP treatments using the hormesis effect because the treatment might result in toxic effects if the dose exceeds the endogenous antioxidant buffering capacity.<sup>36</sup> In other words, the yet unknown “inflection point” must exist somewhere, and the oxidative stress caused by LICAP therapy should not exceed it to achieve a cytoprotective effect. Therefore, to achieve hormesis via LICAP treatment, the plasma density of the device should be precisely tuned to a low range.

Several features of the device used in this study made it possible to enable the generation of low intensity and precisely tuned plasma: (1) radiofrequency (RF) as an energy source, (2) a helical-shaped electrode and gas flow path, and (3) helium as a vehicle gas (Figure 1B). First, it is easier to tune the output energy precisely with the RF method than with the magnetron or arc methods. Second, the device has a helical-shaped RF electrode, whereby the vehicle gas maintains contact with the electrode for as long as possible. Lastly, using helium rather than argon as a vehicle gas increased the efficiency of the procedure.

The LICAP treatment used in this study seems to be an attractive antiaging modality for both dermatologists and patients because it does not ablate the tissue. The results of the present study suggest that LICAP, a CAP with an intensity precisely limited to a low range, can rejuvenate photoaged, wrinkled skin without any destructive damage. However, to develop a LICAP device and its treatment protocol for gentle, effective rejuvenation, identifying the *therapeutic window* becomes a priority, however difficult. A major issue with the latter is that there are limited ways to define *fluence* (energy density,  $J/cm^2$ ), which is a term meant for EBD users to communicate with each other. This is because the form of energy medium of any plasma device is *material* (i.e., the ionized or excited gas molecules and free electrons) whereas that of the conventional EBDs (i.e., laser, RF device, and high-intensity focused ultrasound) is *waveform* (i.e., electromagnetic wave and sound wave). Therefore, unlike other EBDs, the ideal parameter of plasma therapy should be estimated based on the oxidation–reduction status of the target tissue or cell rather than the plasma-generating condition.<sup>17</sup> However, a feasible technique for real-time target monitoring has yet to be developed. We are eager to seek a way to implement it and concurrently develop appropriate treatment protocols based on clinical outcomes.

To the best of our knowledge, the present study is the first to demonstrate the effect of LICAP on UV-induced wrinkles using an animal model; LICAP treatment significantly improved photoaging-induced wrinkles on the dorsal skin of hairless mice. However, this study was limited by the scope of the study which did not reach the estimation of the therapeutic range or the proper treatment protocol for human use. Additionally, the efficacy and safety of LICAP in photoaged human skin should be evaluated in further clinical trials, based on a sufficient review of safety.

In summary, LICAP significantly reduced UV-induced wrinkles in an animal model, and this effect persisted for at least 4 weeks after treatment was discontinued. The data from our histological and in vitro investigations indicate that the improvement of

UV-induced wrinkles is related to the enhanced expression of dermal matrix proteins in human dermal fibroblasts, which shows a hormetic dose–response relationship. The effect of LICAP treatment on UV-induced wrinkles was augmented by the concurrent topical application of the PLA solution. An ideal strategy, such as vehicle gas selection and plasma-generating parameters, for LICAP treatment should be determined when considering the therapeutic window. Further clinical studies are required to confirm these findings.

## ACKNOWLEDGMENTS

This work was supported by the Institute of Information & Communications Technology Planning & Evaluation (IITP) grant funded by the Korean government (MSIT) (No. 2021-0-01074, Development of Intelligent Plasma Medical Device Applying User Data Platform Technology Project).

## CONFLICT OF INTEREST

All authors have completed and submitted the ICMJE Form for disclosure of potential conflicts of interest.

## ORCID

Ga Ram Ahn  <http://orcid.org/0000-0002-5696-4699>

Hyung Joon Park  <http://orcid.org/0000-0002-8803-500X>

Young Gue Koh  <http://orcid.org/0000-0002-6376-0328>

Sun Hye Shin  <http://orcid.org/0000-0002-0479-8174>

Yu Jin Kim  <http://orcid.org/0000-0002-1247-2887>

Min Gyo Song  <http://orcid.org/0000-0002-1530-3480>

Jung Ok Lee  <http://orcid.org/0000-0002-0048-5322>

Kyu Back Lee  <http://orcid.org/0000-0003-2939-5248>

Beom Joon Kim  <http://orcid.org/0000-0003-2320-7621>

## REFERENCES

- Taylor CR, Stern RS, Leyden JJ, Gilchrist BA. Photoaging/photodamage and photoprotection. *J Am Acad Dermatol*. 1990;22(1):1–15. [https://doi.org/10.1016/0190-9622\(90\)70001-x](https://doi.org/10.1016/0190-9622(90)70001-x)
- Scharfetter-Kochanek K, Brenneisen P, Wenk J, et al. Photoaging of the skin from phenotype to mechanisms. *Exp Gerontol*. 2000;35(3):307–16. [https://doi.org/10.1016/s0531-5565\(00\)00098-x](https://doi.org/10.1016/s0531-5565(00)00098-x)
- Zouboulis CC, Ganceviciene R, Liakou AI, Theodoridis A, Elewa R, Makrantonaki E. Aesthetic aspects of skin aging, prevention, and local treatment. *Clin Dermatol*. 2019;37(4):365–72. <https://doi.org/10.1016/j.clindermatol.2019.04.002>
- Metelmann HR, von Woedtke T, Weltmann KD, editors. Comprehensive clinical plasma medicine: cold physical plasma for medical application. Springer International Publishing; 2018. <https://doi.org/10.1007/978-3-319-67627-2>
- Shi X, Cai J, Xu G, Ren H, Chen S, Chang Z, et al. Effect of cold plasma on cell viability and collagen synthesis in cultured murine fibroblasts. *Plasma Sci Technol*. 2016;18(4):353–359. <https://doi.org/10.1088/1009-0630/18/4/04>
- Arndt S, Unger P, Wacker E, Shimizu T, Heinlin J, Li YF, et al. Cold atmospheric plasma (CAP) changes gene expression of key molecules of the wound healing machinery and improves wound healing in vitro and in vivo. *PLoS One*. 2013;8(11):1–9. <https://doi.org/10.1371/journal.pone.0079325>
- Hwang SG, Kim JH, Jo SY, Kim YJ, Won CH. Cold atmospheric plasma prevents wrinkle formation via an antiaging process. *Plasma Med*. 2020;10(2):91–102. <https://doi.org/10.1615/PlasmaMed.2020034810>
- Frescaline N, Duchesne C, Favier M, Onifarasoaniaina R, Guilbert T, Uzan G, et al. Physical plasma therapy accelerates wound re-epithelialisation and enhances extracellular matrix formation in cutaneous skin grafts. *J Pathol*. 2020;252(4):451–64. <https://doi.org/10.1002/path.5546>
- Xu GM, Shi XM, Cai JF, Chen SL, Li P, Yao CW, et al. Dual effects of atmospheric pressure plasma jet on skin wound healing of mice. *Wound Repair Regen*. 2015;23(6):878–84. <https://doi.org/10.1111/wrr.12364>
- Calabrese EJ, Baldwin LA. Hormesis: The dose-response revolution. *Annu Rev Pharmacol Toxicol*. 2003;43(1):175–97. <https://doi.org/10.1146/annurev.pharmtox.43.100901.140223>
- Bustin SA, Beaulieu JF, Huggett J, Jaggi R, Kibenge FS, Olsvik PA, et al. MIQE précis: practical implementation of minimum standard guidelines for fluorescence-based quantitative real-time PCR experiments. *BMC Mol Biol*. 2010;11:74. <https://doi.org/10.1186/1471-2199-11-74>
- Chen Y, Yu Q, Xu CB. A convenient method for quantifying collagen fibers in atherosclerotic lesions by ImageJ software. *Int J Clin Exp Med*. 2017;10(10):14904–10.
- Crowe AR, Yue W. Semi-quantitative determination of protein expression using immunohistochemistry staining and analysis: an integrated protocol. *Bio Protoc*. 2019;9(24). <https://doi.org/10.21769/BioProtoc.3465>
- Holcomb JD, Doolabh V, Lin M, Zimmerman E. High energy, double pass helium plasma dermal resurfacing: a prospective, multicenter, single-arm clinical study. *Lasers Surg Med*. 2022 (January). <https://doi.org/10.1002/lsm.23524>
- Holcomb JD, Kelly M, Hamilton TK, DeLozier JB. A prospective study evaluating the use of helium plasma for dermal resurfacing. *Lasers Surg Med*. 2020;52(10):940–51. <https://doi.org/10.1002/lsm.23257>
- Holcomb JD, Schucker A. Helium plasma skin regeneration: evaluation of skin tissue effects in a porcine model and comparison to nitrogen plasma skin regeneration. *Lasers Surg Med*. 2020;52(1):23–32. <https://doi.org/10.1002/lsm.23167>
- von Woedtke T, Emmert S, Metelmann HR, Ruf S, Weltmann KD. Perspectives on cold atmospheric plasma (CAP) applications in medicine. *Phys Plasmas*. 2020;27(7):070601. <https://doi.org/10.1063/5.0008093>
- Gentile RD. Cool atmospheric plasma (J-plasma) and new options for facial contouring and skin rejuvenation of the heavy face and neck. *Facial Plast Surg*. 2018;34(1):66–74. <https://doi.org/10.1055/s-0037-1621713>
- Privat-Maldonado A, Schmidt A, Lin A, Weltmann KD, Wende K, Bogaerts A, et al. ROS from physical plasmas: Redox chemistry for biomedical therapy. *Oxid Med Cell Longevity*. 2019;2019(ii):1–29. <https://doi.org/10.1155/2019/9062098>
- Szili EJ, Harding FJ, Hong SH, Herrmann F, Voelcker NH, Short RD. The hormesis effect of plasma-elevated intracellular ROS on HaCaT cells. *J Phys D Appl Phys*. 2015;48(49):495401. <https://doi.org/10.1088/0022-3727/48/49/495401>
- Schmidt A, Bekeschus S. Redox for repair: cold physical plasmas and Nrf2 signaling promoting wound healing. *Antioxidants*. 2018;7(10):1–17. <https://doi.org/10.3390/antiox7100146>
- Schmidt A, von Woedtke T, Vollmar B, Hasse S, Bekeschus S. Nrf2 signaling and inflammation are key events in physical plasma-spurred wound healing. *Theranostics*. 2019;9(4):1066–84. <https://doi.org/10.7150/thno.29754>
- Stratmann B, Costea TC, Nolte C, Hiller J, Schmidt J, Reindel J, et al. Effect of cold atmospheric plasma therapy vs standard therapy placebo on wound healing in patients with diabetic foot ulcers: a randomized clinical trial. *JAMA Netw Open*.

- 2020;3(7):e2010411. <https://doi.org/10.1001/jamanetworkopen.2020.10411>
24. Schmidt A, Liebelt G, Striesow J, Freund E, von Woedtke T, Wende K, et al. The molecular and physiological consequences of cold plasma treatment in murine skin and its barrier function. *Free Radic Biol Med.* 2020;161:32–49. <https://doi.org/10.1016/j.freeradbiomed.2020.09.026>
  25. Bellezza I, Giambanco I, Minelli A, Donato R. Nrf2-Keap1 signaling in oxidative and reductive stress. *Biochim Biophys Acta Mol Cell Res.* 2018;1865(5):721–33. <https://doi.org/10.1016/j.bbamcr.2018.02.010>
  26. Kopacz A, Kloska D, Forman HJ, Jozkowicz A, Grochot-Przeczek A. Beyond repression of Nrf2: an update on Keap1. *Free Radic Biol Med.* 2020;157:63–74. <https://doi.org/10.1016/j.freeradbiomed.2020.03.023>
  27. Kang MI, Kobayashi A, Wakabayashi N, Kim SG, Yamamoto M. Scaffolding of Keap1 to the actin cytoskeleton controls the function of Nrf2 as key regulator of cytoprotective phase 2 genes. *Proc Natl Acad Sci.* 2004;101(7):2046–51. <https://doi.org/10.1073/pnas.0308347100>
  28. Velichkova M, Hasson T. Keap1 regulates the oxidation-sensitive shuttling of nrf2 into and out of the nucleus via a crml-dependent nuclear export mechanism. *Mol Cell Biol.* 2005;25(11):4501–13. <https://doi.org/10.1128/mcb.25.11.4501-4513.2005>
  29. Liu WJ, Ye L, Huang WF, Guo LJ, Xu ZG, Wu HL, et al. p62 links the autophagy pathway and the ubiquitin-proteasome system upon ubiquitinated protein degradation. *Cell Mol Biol Lett.* 2016;21(1):29. <https://doi.org/10.1186/s11658-016-0031-z>
  30. Komatsu M, Kurokawa H, Waguri S, Taguchi K, Kobayashi A, Ichimura Y, et al. The selective autophagy substrate p62 activates the stress responsive transcription factor Nrf2 through inactivation of Keap1. *Nat Cell Biol.* 2010;12(3):213–23. <https://doi.org/10.1038/ncb2021>
  31. Jain A, Lamark T, Sjøttem E, Larsen KB, Awuh JA, Øvervatn A, et al. p62/SQSTM1 is a target gene for transcription factor NRF2 and creates a positive feedback loop by inducing antioxidant response element-driven gene transcription. *J Biol Chem.* 2010;285(29):22576–91. <https://doi.org/10.1074/jbc.M110.118976>
  32. Hayashi K, Dan K, Goto F, Tshuchihashi N, Nomura Y, Fujioka M, et al. The autophagy pathway maintained signaling crosstalk with the Keap1-Nrf2 system through p62 in auditory cells under oxidative stress. *Cell Signal.* 2015;27(2):382–93. <https://doi.org/10.1016/j.cellsig.2014.11.024>
  33. Watai Y, Kobayashi A, Nagase H, Mizukami M, McEvoy J, Singer JD, et al. Subcellular localization and cytoplasmic complex status of endogenous Keap1. *Genes Cells.* 2007;12(10):1163–78. <https://doi.org/10.1111/j.1365-2443.2007.01118.x>
  34. Lackmann JW, Wende K, Verlact C, Golda J, Volzke J, Kogelheide F, et al. Chemical fingerprints of cold physical plasmas—an experimental and computational study using cysteine as tracer compound. *Sci Rep.* 2018;8(1):7736. <https://doi.org/10.1038/s41598-018-25937-0>
  35. Sthijns MMJPE, Weseler AR, Bast A, Haenen GRMM. Time in redox adaptation processes: From evolution to hormesis. *Int J Mol Sci.* 2016;17(10):1649. <https://doi.org/10.3390/ijms17101649>
  36. Oliveira MF, Geihs MA, França TFA, Moreira DC, Hermes-Lima M. Is “preparation for oxidative stress” a case of physiological conditioning hormesis? *Front Physiol.* 2018;9:1–6. <https://doi.org/10.3389/fphys.2018.00945>
  37. Choi JH, Nam SH, Song YS, Lee HW, Lee HJ, Song K, et al. Treatment with low-temperature atmospheric pressure plasma enhances cutaneous delivery of epidermal growth factor by regulating E-cadherin-mediated cell junctions. *Arch Dermatol Res.* 2014;306(7):635–43. <https://doi.org/10.1007/s00403-014-1463-9>
  38. Kwon TR, Han SW, Yeo IK, Kim JH, Kim JM, Hong JY, et al. Biostimulatory effects of polydioxanone, poly-d, l lactic acid, and polycaprolactone fillers in mouse model. *J Cosmet Dermatol.* 2019;18(4):1002–08. <https://doi.org/10.1111/jocd.12950>
  39. Lin CY, Lin JY, Yang DY, Lee SH, Kim JY, Kang M. Efficacy and safety of poly-D,L-lactic acid microspheres as subdermal fillers in animals. *Plastic and Aesthetic Research.* 2019;9:16. <https://doi.org/10.20517/2347-9264.2019.23>
  40. Courderot-Masuyer C, Robin S, Tauzin H, Humbert P. Evaluation of the behaviour of wrinkles fibroblasts and normal aged fibroblasts in the presence of poly-L-lactic acid. *J Cosmet Dermatol Sci Appl.* 2012;2(1):20–7. <https://doi.org/10.4236/jcdsa.2012.21006>
  41. Gao Q, Duan L, Feng X, Xu W. Superiority of poly-L-lactic acid) microspheres as dermal fillers. *Chin Chem Lett.* 2020;32:577–82. <https://doi.org/10.1016/j.ccllet.2020.03.071>
  42. Salles AG, Lotierzo PH, Gimenez R, Camargo CP, Ferreira MC. Evaluation of the poly-L-lactic acid implant for treatment of the nasolabial fold: 3-year follow-up evaluation. *Aesthetic Plast Surg.* 2008;32(5):753–756. <https://doi.org/10.1007/s00266-008-9182-2>
  43. No YA, Seok J, Hyun MY, Kwon TR, Oh CT, Choi EJ, et al. Long-term (24-month) safety evaluation of poly-DL-lactic acid filler injection for the nasolabial fold: a multicenter, open, randomized, evaluator-blind, active-controlled design. *Plast Reconstr Surg.* 2015;135(6):1074e–5e. <https://doi.org/10.1097/PRS.0000000000001247>
  44. Narins RS, Baumann L, Brandt FS, Fagien S, Glazer S, Lowe NJ, et al. A randomized study of the efficacy and safety of injectable poly-L-lactic acid versus human-based collagen implant in the treatment of nasolabial fold wrinkles. *J Am Acad Dermatol.* 2010;62(3):448–62. <https://doi.org/10.1016/j.jaad.2009.07.040>
  45. Wen X, Xin Y, Hamblin MR, Jiang X. Applications of cold atmospheric plasma for transdermal drug delivery: a review. *Drug Delivery Transl Res.* 2020;11(37):741–747. <https://doi.org/10.1007/s13346-020-00808-2>
  46. Haralambiev L, Nitsch A, Jacoby JM, Strakeljahn S, Bekeschus S, Mustea A, et al. Cold atmospheric plasma treatment of chondrosarcoma cells affects proliferation and cell membrane permeability. *Int J Mol Sci.* 2020;21(7) <https://doi.org/10.3390/ijms21072291>
  47. Haralambiev L, Nitsch A, Einkenkel R, Muzzio DO, Gelbrich N, Burchardt M, et al. The effect of cold atmospheric plasma on the membrane permeability of human osteosarcoma cells. *Anticancer Res.* 2020;40(2):841–846. <https://doi.org/10.21873/anticancer.14016>
  48. Kaneko T, Sasaki S, Hokari Y, Horiuchi S, Honda R, Kanzaki M. Improvement of cell membrane permeability using a cell-solution electrode for generating atmospheric-pressure plasma. *Biointerphases.* 2015;10(2):029521. <https://doi.org/10.1116/1.4921278>
  49. Yusupov M, van der Paal J, Neyts EC, Bogaerts A. Synergistic effect of electric field and lipid oxidation on the permeability of cell membranes. *Biochim Biophys Acta Gen Subj.* 2017;1861(4): 839–47. <https://doi.org/10.1016/j.bbagen.2017.01.030>
  50. van der Paal J, Verheyen C, Neyts EC, Bogaerts A. Hampering effect of cholesterol on the permeation of reactive oxygen species through phospholipids bilayer: possible explanation for plasma cancer selectivity. *Sci Rep.* 2017;7:1–11. <https://doi.org/10.1038/srep39526>
  51. van der Paal J, Fridman G, Bogaerts A. Ceramide cross-linking leads to pore formation: potential mechanism behind CAP enhancement of transdermal drug delivery. *Plasma Processes Polym.* 2019;16(11):1–10. <https://doi.org/10.1002/ppap.201900122>
  52. Lee HY, Choi JH, Hong JW, Kim GC, Lee HJ. Comparative study of the Ar and He atmospheric pressure plasmas on E-cadherin protein regulation for plasma-mediated transdermal drug delivery. *J Phys D Appl Phys.* 2018;51(21):215401. <https://doi.org/10.1088/1361-6463/aab8dc>

53. Joh HM, Kim SJ, Chung TH, Leem SH. Comparison of the characteristics of atmospheric pressure plasma jets using different working gases and applications to plasma-cancer cell interactions. *AIP Adv.* 2013;3(9):0–12. <https://doi.org/10.1063/1.4823484>

### SUPPORTING INFORMATION

Additional supporting information can be found online in the Supporting Information section at the end of this article.

**How to cite this article:** Ahn GR, Park HJ, Koh YG, Shin SH, Kim YJ, Song MG, et al. Low-intensity cold atmospheric plasma reduces wrinkles on photoaged skin through hormetic induction of extracellular matrix protein expression in dermal fibroblasts. *Lasers Surg Med.* 2022;54:978–993. <https://doi.org/10.1002/lsm.23559>